ceramics

MDPI

Article

Effect of Synthetic Approaches and Sintering Additives upon Physicochemical and Electrophysical Properties of Solid Solutions in the System $(CeO_2)_{1-x}(Nd_2O_3)_x$ for Fuel Cell Electrolytes

Marina V. Kalinina [1], Daria A. Dyuskina [1], Irina G. Polyakova [1], Sergey V. Mjakin [2,3,*] and Irina Yu. Kruchinina [1,4]

[1] Institute of Silicate Chemistry of the Russian Academy of Sciences, 2 Makarova Emb, 199034 St. Petersburg, Russia
[2] Department of Theory of Materials Sciences, Saint-Petersburg State Institute of Technology, Technical University, 24-26/49A Moskovsky Prospect, 190013 St. Petersburg, Russia
[3] Institute for Analytical Instrumentation, Russian Academy of Sciences, 31-33A Ivana Chernykh Str., 198095 St. Petersburg, Russia
[4] Department of Nanotechnology and Nanomaterials for Radioelectronics, Saint-Petersburg State Electrotechnical University "LETI", 5 Professora Popova Str., 197376 St. Petersburg, Russia
* Correspondence: svmjakin@technolog.edu.ru

Abstract: Finely dispersed $(CeO_2)_{1-x}(Nd_2O_3)_x$ (x = 0.05, 0.10, 0.15, 0.20, 0.25) powders are synthesized via liquid-phase techniques based on the co-precipitation of hydroxides and co-crystallization of nitrates. The prepared powders are used to obtain ceramic materials comprising fluorite-like solid solutions with the coherent scattering region (CSR) of about 88 nm (upon annealing at 1300 °C) and open porosity in the range of 1–15%. The effect of the synthesis procedure and sintering additives (SiO_2, ZnO) on physicochemical and electrophysical properties of the resulting ceramics is studied. The prepared materials are found to possess a predominantly ionic type of electric conductivity with ion transfer numbers t_i = 0.96–0.71 in the temperature range of 300–700 °C. The conductivity in solid solutions follows a vacancy mechanism with $\sigma_{700\,^\circ C} = 0.48 \times 10^{-2}$ S/cm. Physicochemical properties (density, open porosity, type and mechanism of electrical conductivity) of the obtained ceramic materials make them promising as solid oxide electrolytes for medium temperature fuel cells.

Keywords: co-precipitation; co-crystallization; oxides; finely dispersed powders; nanoceramics; density; porosity; fuel cells; electrolytes

Citation: Kalinina, M.V.; Dyuskina, D.A.; Polyakova, I.G.; Mjakin, S.V.; Kruchinina, I.Y. Effect of Synthetic Approaches and Sintering Additives upon Physicochemical and Electrophysical Properties of Solid Solutions in the System $(CeO_2)_{1-x}(Nd_2O_3)_x$ for Fuel Cell Electrolytes. *Ceramics* **2023**, *6*, 1100–1112. https://doi.org/10.3390/ceramics6020065

Academic Editors: Gilbert Fantozzi and Narottam P. Bansal

Received: 3 March 2023
Revised: 17 April 2023
Accepted: 8 May 2023
Published: 11 May 2023

1. Introduction

In view of unstable situation on the market of hydrocarbon resources and growing environmental problems, the power supply sector is undergoing significant structural changes, particularly involving the increase in the use of alternative (relating to conventionally applied timber, coal and oil) resources, opening new prospects for the development of energy generation, accumulation and distribution systems. Particularly promising are fuel cells (FC)—electrochemical devices directly converting the chemical energy of the fuel and oxidizer separately supplied to electrodes into electric power. A high thermodynamic efficiency and a permanent and environment friendly operation make FCs advantageous over such power generation systems as microturbines, internal combustion engines and solar cells [1–5].

The application of solid oxide fuel cells (SOFCs) affords the development of various scale and purpose installations from portative to high power stationary ones. Medium temperature SOFC operate at 300–700 °C that provides their high (50–70%) power efficiency, reduction of risks relating to electrode catalyst poisoning and increased rate of electrode reactions. SOFs are also promising in respect of their enhanced tolerance to impurities in the fuel and versatility of applied combustible gases compared with other types of

FCs [6–8]. Furthermore, SOFCs are full-ceramic systems causing no adverse impact on the environment. The current trends in the development of SOFCs and high research activity in this field indicate prospects for their extensive commercialization in the nearest years.

According to the above considerations, a promising research area relates to the development of components for medium temperature solid oxide fuel cells (MT-SOFC) applicable for electric power generation using a synthesis gas (H_2-CO) fuel obtained from any hydrocarbons. The most promising material for solid electrolytes in MT-SOFC is cerium dioxide (ceria) doped with oxides of rare-earth elements (REE). Nanoscale CeO_2 based electrolytes provide electric performances comparable with conventionally used zirconia and allow a significant reduction of working temperature for fuel cells, thus increasing their durability [9,10].

Different kinds of FCs being currently developed are classified primarily according to the type of applied electrolytes, particularly divided by ion transport mechanisms to anionic, protonic and mixed ion types. MT-SOFC operation is based on the transport of oxygen ions (O^{2-}) from cathode to anode. Since this mechanism requires the presence of oxygen vacancies, electrolytes useful for these systems should contain anionic vacancies in the crystal lattice [11–13]. Furthermore, to obtain solid electrolytes with optimal exploration performances (ionic conductivity, gas tightness, thermal stability, mechanical strength), fine powders are required [11,12].

The electric performance of CeO_2-REE electrolytes depends on numerous factors including the applied synthetic approach, dispersion of the prepared precursor powders, ceramic density and grain size [8,14–17].

The preparation of ceramic materials with a certain density requires the proper choice of the precursor powder synthesis procedure and analysis of the prepared powder consolidation, involving the steps of compression (compacting) and subsequent sintering. One of the most important procedures in the ceramic preparation technology is annealing to provide the material sintering. In order to accelerate the sintering process, reduce the sintering temperature and improve the target performances of the resulting ceramics, so called sintering additives are used to promote the intensification of physicochemical processes in the course of annealing. Both specially introduced additives and even admixtures in the applied reagents are known to affect the formation and sintering temperatures of the prepared compounds, as well as their physical, chemical and technical performances. The effect of each additive is determined by a certain specific mechanism [18].

The most preferable approaches to obtaining precursor powders for ceramics involve such liquid-phase methods as hydrothermal synthesis, the sol-gel method, Pechini method, the co-precipitation of hydroxides from solutions of inorganic salts, and the co-crystallization of salts. A particularly promising one is the co-precipitation of hydroxides followed by low-temperature treatment, providing a more precise adjustment of the dispersion and microstructure of the target products due to the variation of the synthesis conditions and obtaining single phase xerogels and powders with a required composition and high specific surface area [19–21].

The compression of ceramics largely depends on the controlled introduction of additives, significantly affecting the consolidation even in very small contents. For example, some additives can provide a decisive effect on the compression in the course of sintering, resulting in an increase in the mechanical strength of porous ceramics, as well as in the reduction of the sintering temperature upon the addition in the amount of 10^{-2} %wt. The action mechanism of such additives is different and is determined by the nature of the base material and the additive, as well as by their high-temperature interaction. Additives can activate the sintering process by blocking the growth of grains, being localized at the grain boundaries.

The aim of this research Is the study of the effect of synthetic approaches and sintering additives (SiO_2 and ZnO) upon physicochemical and electrophysical properties of solid solutions in the system $(CeO_2)_{1-x}(Nd_2O_3)_x$ for MT-SOFC electrolytes.

2. Materials and Methods

2.1. Synthesis of $(CeO_2)_{1-x}(Nd_2O_3)_x$ (x = 0.05, 0.10, 0.15, 0.20, 0.25)

The precursor powders were synthesized using two different methods, including co-precipitation of hydroxides followed by low temperature treatment and co-crystallization of nitrates, providing various CeO_2:Nd_2O_3 ratios in both cases.

For the synthesis, nitric acid salts of cerium $Ce(NO_3)_3 \cdot 6H_2O$ (analytical purity grade with the reagent content higher than 98 %wt.) and neodymium $Nd(NO_3)_3 \cdot 6H_2O$ (chemical purity grade with the reagent content higher than 99 %wt.) were used, from which diluted (~0.1 M) solutions were prepared.

In the case of the co-precipitation of hydroxides, the precursor powder synthesis was carried out by reverse titration followed by low temperature treatment. A 1 M aqueous solution of ammonia hydrate ($NH_3 \cdot H_2O$) was used as a precipitating agent. The pH of the reaction mixture was maintained on level 11–12. The precipitation was performed with a minimal rate of 0.02 cm^3/s at thorough mixing. The prepared gelatinous precipitate of hydroxides was filtered followed by freezing at −25 °C within 24 h to provide deagglomeration and maintain a fine dispersion of the CeO_2–Nd_2O_3 co-precipitate.

The co-crystallization procedure was carried out by the evaporation of water from the solutions on a water bath within 3 h to obtain supersaturated solutions. Then the resulting supersaturated solutions were cooled at 3–5 °C to promote the adsorption of the crystallized compounds on the surface of the crystals formed during the evaporation.

The xerogels obtained by both methods were dried at 120 °C within 1 h followed by heating at 600 °C within 1 h to form nanopowders with a stable crystal structure. Then sintering additives (SiO_2 or ZnO) were introduced to the prepared nanopowders in the amount of 3 %wt. relating to the powder charge weight [21].

The prepared powders in the amount of 1.5–2.0 g were consolidated into tablets (diameter 1.5 cm, height 0.2–0.4 cm) by single-axis cold compression in a steel mold under a pressure of 150 MPa by isostatic cold pressing, followed by sintering at 1300 °C in air, with the heating rate and furnace cooling 7 °C/min.

2.2. Characterization Methods

X-ray diffraction analysis (XRD) was performed using a D8-Advanse diffractometer (Bruker, Billerica, MA, USA), CuK_α radiation, 2θ = 15–60°, in air. The international database ICDD-2006 was used to interpret the diffraction patterns; the analysis results were processed using the WINFIT 1.2.1 software using the Fourier transform of the reflex profile. The size of coherent scattering regions (CSR) was estimated using a Selyakov-Scherrer equation:

$$D_{CSR} = 0.9 \cdot \lambda / (\beta \cdot \cos\theta)$$

where λ is the CuKα wavelength and β is the diffraction peak FWHM. CSR was estimated on the basis of changes in XRD reflection profiles with changes in the grain size [22].

The open porosity was measured by hydrostatic weighting in distilled water according to the Russian standard GOST 473.4-81 [23].

The surface functionality of the prepared samples was studied using a dynamic pH-metry technique [24,25]. The acid-base properties of the powder surface were characterized by measuring the changes in pH value of the suspensions obtained by immersing 30 mg of the studied powders in 30 mL of distilled water at permanent agitation with a magnetic stirrer. pH measurements were performed using a Multitest IPL-301 pH-meter (NPP SEMICO, Novosibirsk, Russia) in 5, 10, 20, 30, 40, 50, 60 s after the sample immersion and subsequently in every 30 s up to 10 min from the powder immersion.

The electrical resistance of the obtained ceramic materials was measured by a two-contact method at direct current using the "Hardware-software installation for investigating the electrical properties of nanoceramics in different gas media" [26]. To provide electrical contact, silver electrodes were applied to the ends of the measured samples by annealing a silver conductive paste. After drying the paste, the samples were slowly heated to 600 °C

and held for 1 h at this temperature to burn out the organic components, followed by slow cooling. The conductivity of ceramics was measured in the temperature range from 250 to 900 °C, because heating to higher temperatures can lead to the melting of the silver contacts.

The obtained materials generally feature a semiconductor type (increase with temperature) and ionic mechanism of electrical conductivity according to the following quasi-chemical reaction:

$$Nd_2O_3 \xrightarrow{CeO_2} 2Nd'_{Ce} + 3O^x_o + V$$

where Nd'_{Ce} is a neodymium ion replacing Ce^{4+} and $V_{ö}$ is oxygen vacancy.

The transfer numbers of ions and electrons in bulky solid electrolytes were determined by the West–Tallan method [19] using a CO_2 + CO mixture (corresponding to an oxygen partial pressure of 10^3 Pa) as an inert gas. The measurements were carried out using a direct current in weak (U = 0.5 V) fields after a long (up to 30 min) drop of the current. The contributions of ionic and electronic conductivity were estimated as:

$$t_e = R_{air}/R_e$$

and

$$t_i = 1 - t_e$$

where t_e and t_i are the transport numbers of electrons and ions, respectively, R_{air} and R_e are the sample resistance measured in air and in an inert gas atmosphere.

The resulting ceramics microstructure was characterized using a Tescan Amber GMH (Tescan, Chech Respublic) electron microscope with the secondary electron detector (Everhard-Tornley) at magnification 75,000×.

3. Results and Discussion

3.1. Study of the $(CeO_2)_{1-x}(Nd_2O_3)_x$ (x = 0.05; 0.10; 0,15; 0,20; 0,25) Solid Solutions Crystal Structure

XRD results for the $(CeO_2)_{0.85}(Nd_2O_3)_{0.15}$ precursor powder synthesized by the co-precipitation of hydroxides and annealed at 600 °C, as well as the ceramics sample obtained by its subsequent sintering at 1300 °C (Figure 1 and Table 1), indicate the formation of finely dispersed solid solutions with the fluorite-like cubic structure. For the nanopowder annealed at 600 °C, the lattice parameter a = 5.4360 Å and CSR ~ 14 nm, while after sintering at 1300 °C, a = 5.4545 Å and CSR = 88 nm. Thus, the resulting ceramics feature a single-phase structure in the temperature range 600–1300 °C. The effect of the dopant concentration upon the cubic solid solution formation XRD profiles for all the studied $(CeO_2)_{1-x}(Nd_2O_3)_x$ compositions (x = 0.05; 0.10; 0.20; 0.25) is shown in Figure 2 and Table 2.

Table 1. XRD parameters of $(CeO_2)_{0.85}(Nd_2O_3)_{0.15}$ ceramics annealed at 1300 °C.

2θ, °	d_{hkl}	I	hkl Indices	Cubic Lattice Parameter, Å	Structure
28.4453	3.14930	296.0	111	5.4545	Fm3m
32.9427	2.72737	88.9	200		
47.0850	1.92854	137.9	220		
55.8549	1.64467	101.1	311		
58.5220	1.57465	28.3	222		
68.7800	1.36369	20.1	400		

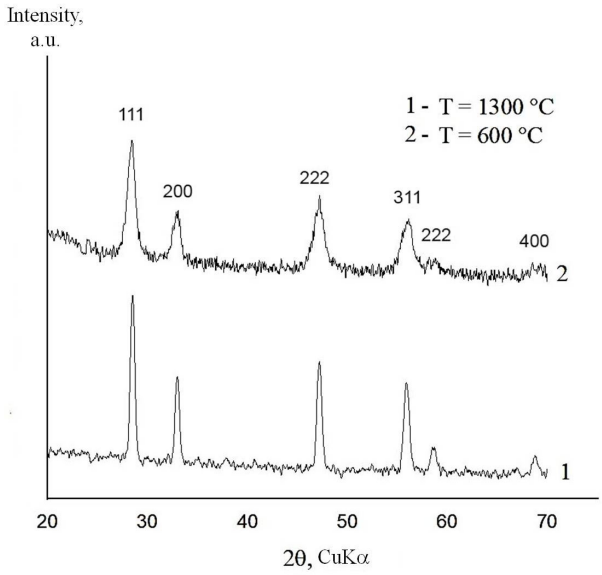

Figure 1. XRD profiles for $(CeO_2)_{0.85}(Nd_2O_3)_{0.15}$ precursor nanopowder (1) and ceramic sample (2) prepared by co-precipitation of cerium and neodymium hydroxides.

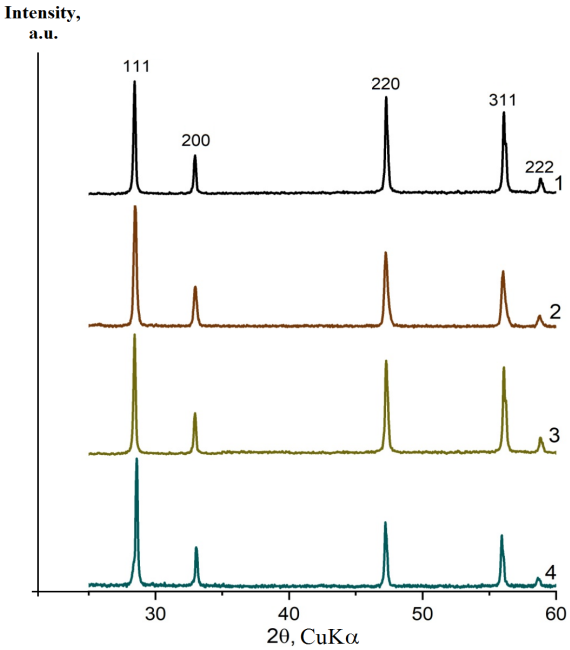

Figure 2. XRD profiles for $(CeO_2)_{0.85}(Nd_2O_3)_{0,15}$ ceramics samples with x = 0.05 (1), 0.10 (2), 0.20 (3) and 0.25 (4) synthesized by co-precipitation of hydroxides followed by annealing at 1300 °C.

Table 2. Cubic lattice parameters and CSR value for $(CeO_2)_{1-x}(Nd_2O_3)_x$ (x = 0.05, 0.10, 0.20 and 0.25) ceramic samples.

Composition	Structure, Parameter a, Å	CSR, nm (1300 °C)
$(CeO_2)_{0.95}(Nd_2O_3)_{0.05}$	F, a = 5.4345	90
$(CeO_2)_{0.90}(Nd_2O_3)_{0.10}$	F, a = 5.4421	89
$(CeO_2)_{0.85}(Nd_2O_3)_{0.15}$	F, a = 5.4545	88
$(CeO_2)_{0.80}(Nd_2O_3)_{0.20}$	F, a = 5.4575	85
$(CeO_2)_{0.75}(Nd_2O_3)_{0.25}$	F, a = 5.4653	81

According to Figure 2, all XRD profiles are similar and correspond to the cubic fluorite-like structure.

The cubic lattice parameters depending on $(CeO_2)_{1-x}(Nd_2O_3)_x$ solid solution composition, as well as the corresponding CSR values are summarized in Table 2.

As shown in Table 2, the concentration of Nd_2O_3 additive in the studied range does not cause any change in the cubic solid solution type, resulting only in a slight increase in the lattice parameter with Nd_2O_3 content and CSR variation in the range of 81–90 nm.

The annealed (1300 °C) ceramics microstructure features prominent 200–700 nm sized grains with well-defined boundaries intrinsic to ceramic samples (Figure 3).

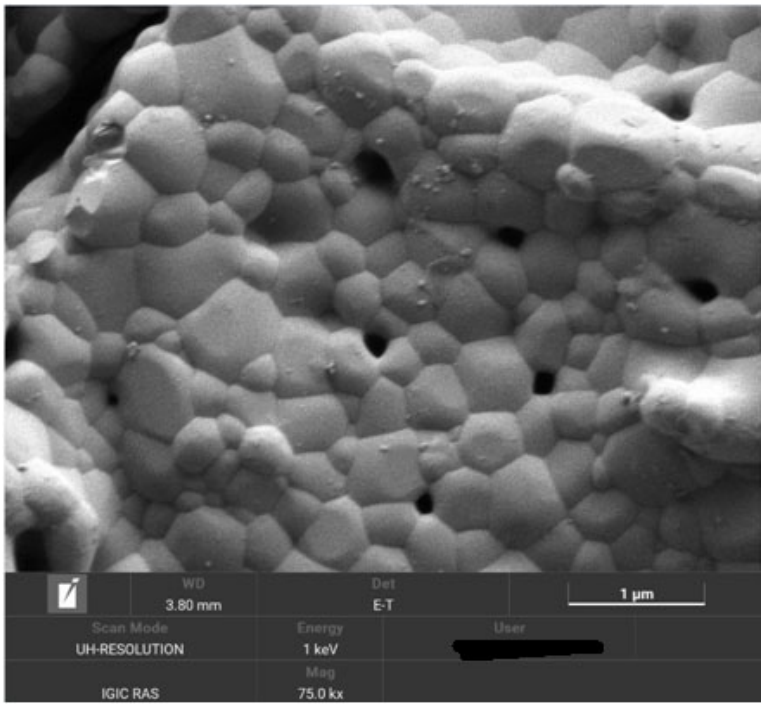

Figure 3. SEM image of $(CeO_2)_{0.90}$ $(Dy_2O_3)_{0.10}$ ceramics sample.

The density and porosity of all the CeO_2-Nd_2O_3 ceramics samples synthesized by both co-precipitation and co-crystallization methods are summarized in Table 3.

Table 3. Effect of sintering additives upon theoretical density ρ, apparent density ρ_a and open porosity P_o of $(CeO_2)_{1-x}(Nd_2O_3)_x$ samples prepared by co-precipitation and co-crystallization.

Composition	ρ, g/cm^3	ρ_a, g/cm^3	P_o, %	Composition	ρ, g/cm^3	ρ_a, g/cm^3	P_o, %
Co-Precipitation				**Co-Crystallization**			
Without sintering additives							
$(CeO_2)_{0.95}(Nd_2O_3)_{0.05}$	5.59	5.47	23.9	$(CeO_2)_{0.95}(Nd_2O_3)_{0.05}$	6.49	6.31	9.7
$(CeO_2)_{0.90}(Nd_2O_3)_{0.10}$	4.84	4.67	29.9	$(CeO_2)_{0.90}(Nd_2O_3)_{0.10}$	5.91	5.76	20.5
$(CeO_2)_{0.85}(Nd_2O_3)_{0.15}$	4.86	4.74	29.4	$(CeO_2)_{0.85}(Nd_2O_3)_{0.15}$	6.47	5.69	25.9
$(CeO_2)_{0.80}(Nd_2O_3)_{0.20}$	6.32	6.16	16.2	$(CeO_2)_{0.80}(Nd_2O_3)_{0.20}$	5.86	5.60	25.8
$(CeO_2)_{0.75}(Nd_2O_3)_{0.25}$	5.32	5.11	21.8	$(CeO_2)_{0.75}(Nd_2O_3)_{0.25}$	5.29	5.06	34.2
With SiO_2 sintering additive							
$(CeO_2)_{0.95}(Nd_2O_3)_{0.05}$	6.12	5.57	23.5	$(CeO_2)_{0.95}(Nd_2O_3)_{0.05}$	5.35	5.14	24.6
$(CeO_2)_{0.90}(Nd_2O_3)_{0.10}$	6.32	4.30	32.9	$(CeO_2)_{0.90}(Nd_2O_3)_{0.10}$	4.95	4.81	31.1

Table 3. *Cont.*

Composition	ρ, g/cm^3	ρ$_a$, g/cm^3	P$_o$, %	Composition	ρ, g/cm^3	ρ$_a$, g/cm^3	P$_o$, %
Co-Precipitation				**Co-Crystallization**			
$(CeO_2)_{0.85}(Nd_2O_3)_{0.15}$	6. 25	4.53	23.8	$(CeO_2)_{0.85}(Nd_2O_3)_{0.15}$	6.41	4.78	33.2
$(CeO_2)_{0.80}(Nd_2O_3)_{0.20}$	6.31	4.13	29.6	$(CeO_2)_{0.80}(Nd_2O_3)_{0.20}$	5.37	4.18	40.7
$(CeO_2)_{0.75}(Nd_2O_3)_{0.25}$	4.81	4.69	25.6	$(CeO_2)_{0.75}(Nd_2O_3)_{0.25}$	4.64	3.98	44.3
With ZnO sintering additive							
$(CeO_2)_{0.95}(Nd_2O_3)_{0.05}$	6.32	6.25	10.1	$(CeO_2)_{0.95}(Nd_2O_3)_{0.05}$	6.70	6.41	0.6
$(CeO_2)_{0.90}(Nd_2O_3)_{0.10}$	6.65	6.52	15.5	$(CeO_2)_{0.90}(Nd_2O_3)_{0.10}$	7.15	7.02	3.4
$(CeO_2)_{0.85}(Nd_2O_3)_{0.15}$	6.26	6.21	13.5	$(CeO_2)_{0.85}(Nd_2O_3)_{0.15}$	6.85	6.62	6.5
$(CeO_2)_{0.80}(Nd_2O_3)_{0.20}$	7.12	6.97	9.9	$(CeO_2)_{0.80}(Nd_2O_3)_{0.20}$	6.62	6.54	0.6
$(CeO_2)_{0.75}(Nd_2O_3)_{0.25}$	6. 56	6.38	14.0	$(CeO_2)_{0.75}(Nd_2O_3)_{0.25}$	4.58	6.52	1.0

3.2. Characterization of the Powders Surface Properties by Dynamic pH-Metry

The data shown in Figure 4 indicate that the immersion of the additive-free CeO_2 in water leads to a small (by about 0.02–0.03) pH decrease within 2.5 min followed by the growth up to the initial level in 4–5 min, suggesting a relatively passive state of the surface with a low content of active sites. The addition of 10% Nd results in a slight change in pH change kinetics with a more prominent (by 0.04) decrease in pH value in the first 2–2.5 min and a similar increase to the initial level. The increase of Nd content to 20% leads to a qualitatively similar but significantly more prominent pH changes including a drop by 0.08 within the first minute followed by a gradual increase to the value exceeding the initial level by 0.08.

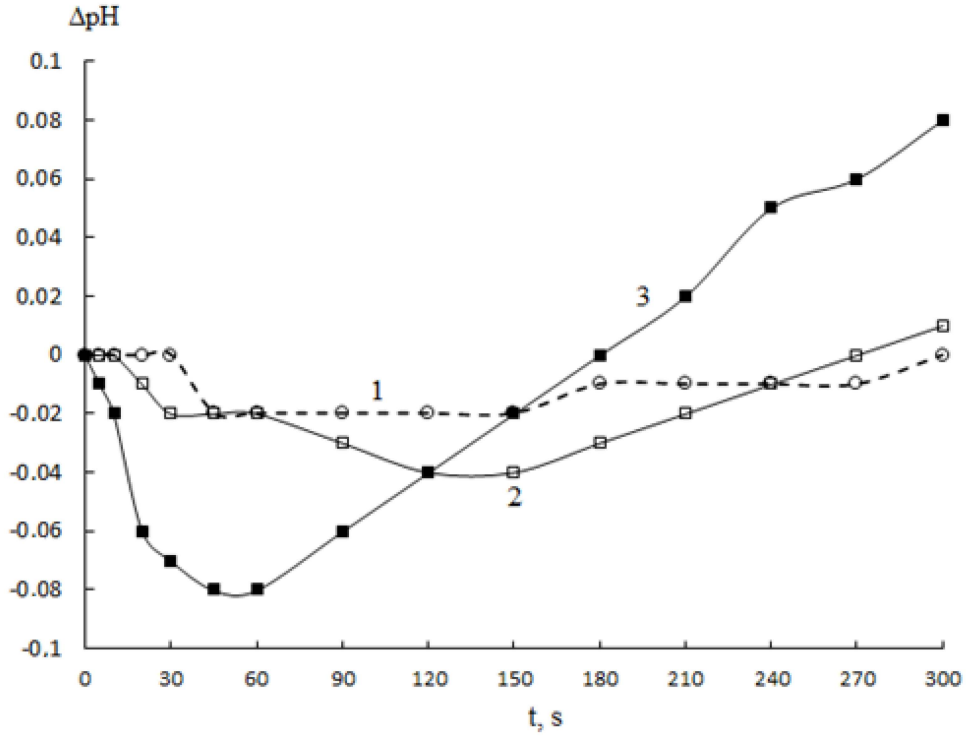

Figure 4. pH changes with time in suspensions of (1) CeO_2, (2) $(CeO_2)_{0.95}(Nd_2O_3)_{0.05}$ and (3) $(CeO_2)_{0.80}(Nd_2O_3)_{0.20}$.

The observed pH changes in aqueous suspensions can be accounted for in the following mechanism. The decrease in pH value within the first minutes after the samples immersion can be determined by the presence of Lewis (metal cations) and Broensted (OH-groups dissociating with proton release) acidic centers, while the subsequent pH growth is likely caused by Broensted basic centers (hydroxyls slowly dissociating with the release of the whole OH-group). Broensted acidic and basic centers can be represented by the groups M-OH and $M(OH)_2$ (M = Ce, Nd), respectively. The addition of neodimium probably results in a distortion of element-oxygen bridging bonds on the surface yielding both types of such centers in the amount growing with the increase in Nd content. The formation of Broensted acidic and basic centers can facilitate ceramics consolidation due to their condensation resulting in the formation of oxygen bridging bonds between neighboring particles.

3.3. Electrical Properties of $(CeO_2)_{1-x}(Nd_2O_3)_x$ (x = 0.05, 0.10, 0.15, 0.20, 0.25) Ceramics

The data on specific conductivity of $(CeO_2)_{0.90}(Nd_2O_3)_{0.1}$ ceramics containing 3 %wt. of SiO_2 and ZnO sintering additives are shown in Figure 5 in comparison with a similar additive-free material. All the samples feature an increase in conductivity with temperature, suggesting a semiconductor type of conductivity. The addition of silica leads to a decrease in conductivity in the entire studied temperature range, probably due to an increased porosity. The addition of zinc oxide also results in a drop in the conductivity at low temperatures, but at elevated temperatures, the conductivity significantly grows and exceeds the values for the additive-free samples.

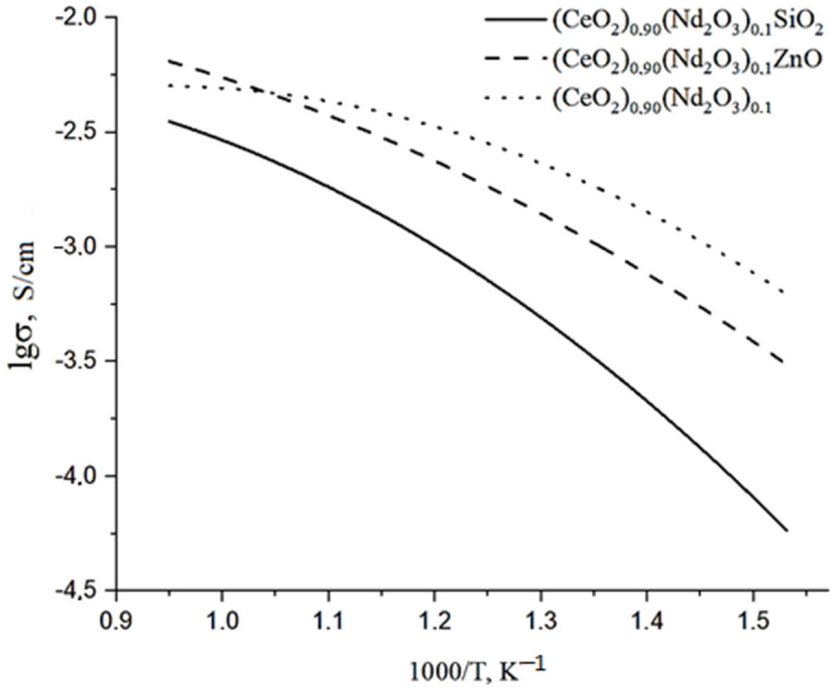

Figure 5. Effect of SiO_2 and ZnO sintering additives on the temperature dependence of $(CeO_2)_{0.90}(Nd_2O_3)_{0.1}$ ceramics conductivity.

Thus, it can be concluded that the use of ZnO as a sintering additive provides both a reduction in porosity and increase in specific conductivity. Therefore, all the subsequent studies were carried out using ZnO-containing samples.

The comparison of specific conductivity vs. temperature plots for the samples with different Nd_2O_3 contents synthesized by the co-precipitation of hydroxides and co-crystallization of salts is presented in Figure 6.

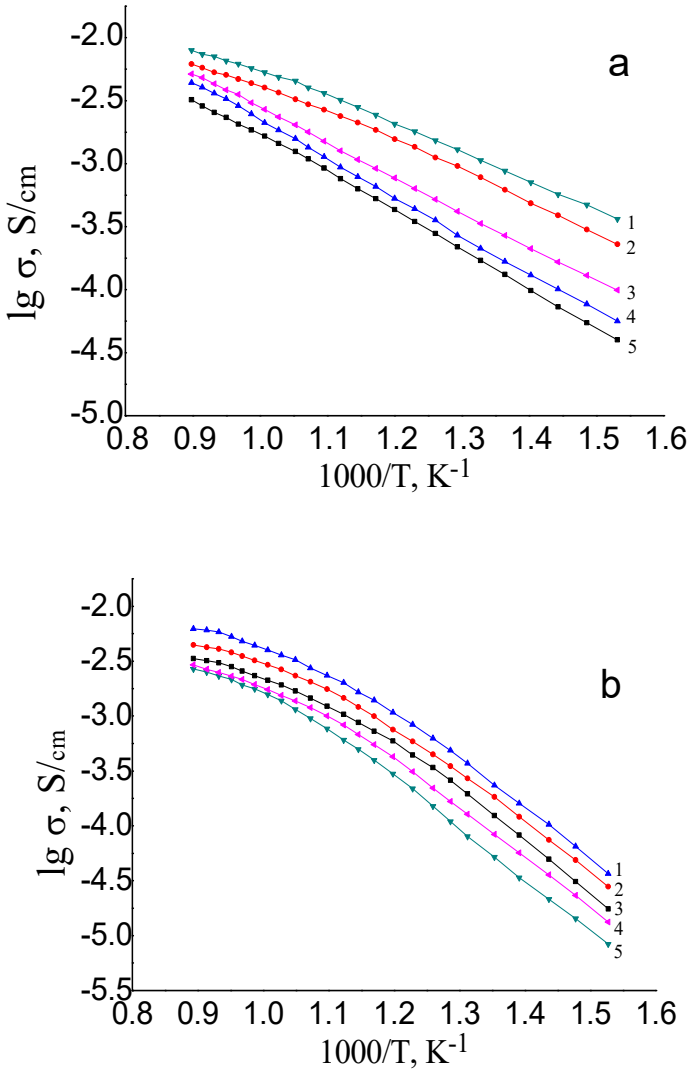

Figure 6. Specific conductivity vs. temperature plots for $(CeO_2)_{1-x}(Nd_2O_3)_x$ ceramics prepared using ZnO sintering additive by (**a**) co-precipitation with x = 0.15 (1), 0.10 (2), 0.25 (3), 0.20 (4), 0.05 (5) and (**b**) co-crystallization with x = 0.15 (1), 0.10 (2), 0.20 (3), 0.05 (4), 0.25 (5).

These data indicate that the highest conductivity is observed for the samples containing 10–15 %wt. Nd_2O_3. The further increase in Nd_2O_3 content leads to a decrease in conductivity, probably due to the formation of "quasi-chemical complexes" $(Nd'_{Ce}–V_O^{\bullet\bullet})^{\bullet}$ involving Nd^{3+} ions and oxygen vacancies $V_O^{\bullet\bullet}$ [8]. Consequently, the concentration of mobile oxygen vacancies drops upon the increase of Nd content above the optimal value, resulting in the observed decrease in specific conductivity.

These data indicate that the highest conductivity is observed for the samples containing 10–15 %wt. Nd_2O_3. The further increase of Nd_2O_3 content leads to a decrease in conductivity, probably due to the formation of "quasi-chemical complexes" $(Nd'_{Ce} –V_O^{\bullet\bullet})^{\bullet}$ involving Nd^{3+} ions and oxygen vacancies $V_O^{\bullet\bullet}$ [8]. Consequently, the concentration of mobile oxygen vacancies drops upon the increase in Nd content above the optimal value, resulting in the observed decrease in specific conductivity.

For comparison, the specific conductivity values at the same temperature 700 °C for the samples synthesized using different methods are shown in Table 4.

Table 4. Specific conductivity of the samples prepared by different methods at 700 °C.

Composition	Specific Conductivity, $\sigma_{700\,^{\circ}C} \cdot 10^{-2}$, S/cm	
	Co-Precipitation	Co-Crystallization
$(CeO_2)_{0.95}(Nd_2O_3)_{0.05}$	0.14	0.15
$(CeO_2)_{0.90}(Nd_2O_3)_{0.10}$	0.36	0.26
$(CeO_2)_{0.85}(Nd_2O_3)_{0.15}$	0.48	0.35
$(CeO_2)_{0.80}(Nd_2O_3)_{0.20}$	0.18	0.19
$(CeO_2)_{0.75}(Nd_2O_3)_{0.25}$	0.22	0.14

The effect of synthetic procedure on the conductivity of $(CeO_2)_{0.75}(Nd_2O_3)_{0.25}$ ceramics containing 3 %wt. ZnO in the temperature range 250–900 °C is illustrated in Figure 7.

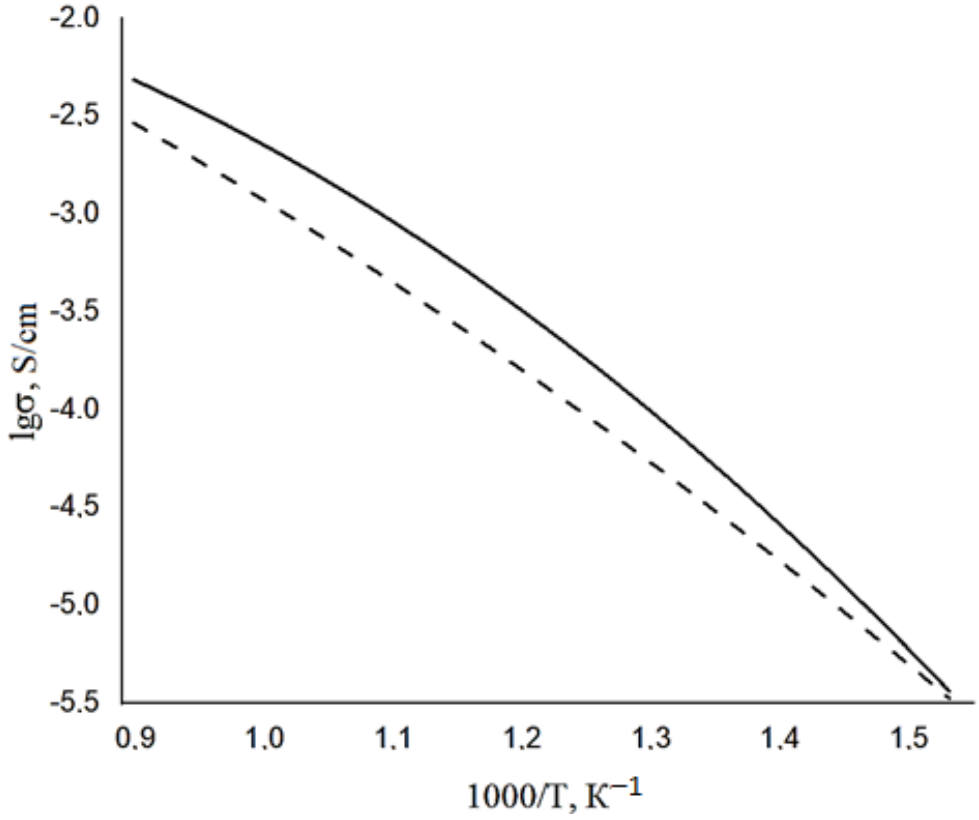

Figure 7. Specific conductivity of $(CeO_2)_{0.75}(Nd_2O_3)_{0.25}$ ceramics prepared by coprecipitation (——) and co-crystallization (- - -) and containing 3 %wt. ZnO as a function of temperature.

These comparative data show that higher specific conductivity is achieved for the samples prepared by co-precipitation, probably because this method provides more finely dispersed powders and consequently ceramics with higher density-based thereon.

The transport numbers of ions (t_i) and electrons (t_e) corresponding to the contributions of electron and ionic components in the overall conductivity were determined using the West-Tallan method and summarized in Table 5. The analysis of these data indicates that the prepared solid oxide electrolytes feature a mixed type of conductivity with the overall predominance of the ionic component and growth of the electronic component with temperature increase. The transport number of ions in the temperature range 300–700 °C is t_i = 0.93–0.66 and the average conductivity at 700 °C is $\sigma_{700^{\circ}C} = 0.47 \times 10^{-2}$ S/cm.

Table 5. Transport numbers of ions and electrons in the synthesized ceramics samples.

Composition	Preparation Method	T. °C	t_i	t_e
$(CeO_2)_{0.95}(Nd_2O_3)_{0.05}$	co-precipitation	400	0.85	0.15
		700	0.83	0.18
$(CeO_2)_{0.90}(Nd_2O_3)_{0.10}$	co-precipitation	400	0.93	0.07
		700	0.85	0.15
$(CeO_2)_{0.85}(Nd_2O_3)_{0,15}$	co-precipitation	400	0.96	0.04
		700	0.84	0.16
$(CeO_2)_{0.95}(Nd_2O_3)_{0.05}$	co-crystallization	700	0.85	0.15
		700	0.71	0.29
$(CeO_2)_{0.90}(Nd_2O_3)_{0.10}$	co-crystallization	400	0.87	0.13
		700	0.78	0.22
$(CeO_2)_{0.85}(Nd_2O_3)_{0.15}$	co-crystallization	400	0.89	0.11
		700	0.74	0.26

4. Conclusions

There is a series of finely dispersed powders in the system $(CeO_2)_{1-x}(Nd_2O_3)_x$ (x = 0.05, 0.10, 0.20, 0.25) with CSR ~ 14 nm. The consolidation of the prepared precursor powders provided ceramic materials with a fluorite-like structure, CSR 88 nm (1300 °C), open porosity in the range of 0.6–15.5% and apparent density od 7.02–6.21 g/cm^3.

The addition of neodymium oxide to ceria imparts the surface with increased Broensted acid-base properties corresponding to the presence of acidic and basic hydroxyls that can facilitate the ceramics sintering due to the formation of oxygen bridging bonds in the course of sintering.

The comparative characterization of ceramic samples sintered with and without SiO_2 and ZnO additives revealed that the addition of ZnO provided the lowest porosity and highest density while the use of SiO_2 as a sintering additive deteriorated these properties towards the porosity growth and density reduction.

The electrical conductivity in CeO_2-Nd_2O_3 solid solutions is found to proceed according to the vacancy mechanism with the predominance of ionic conductivity characterized by the transport number of ions t_i = 0.96–0.71 in the temperature range 300–700 °C and the average conductivity at 700 °C $\sigma_{700\,^\circ C} = 0.47 \times 10^{-2}$ S/cm. The best conductivity performances are achieved for the sample $(CeO_2)_{0.85}(Nd_2O_3)_{0.15}$ prepared by co-precipitation and containing 3 %wt. ZnO as a sintering additive.

According to their mechanical (density, open porosity) and electrophysical (conductivity value, type and mechanism) properties, the obtained ceramic electrolyte materials are promising as components of solid oxide medium temperature fuel cells.

Author Contributions: Conceptualization, M.V.K.; methodology, M.V.K. and I.G.P.; validation, M.V.K., D.A.D. and S.V.M.; formal analysis, M.V.K., I.G.P. and S.V.M.; investigation, M.V.K., D.A.D., I.G.P. and S.V.M.; resources, M.V.K. and I.Y.K.; data curation, M.V.K., I.G.P., S.V.M. and D.A.D.; writing—original draft preparation, M.V.K.; writing—review and editing, M.V.K. and S.V.M.; visualization, D.A.D. and S.V.M.; supervision, M.V.K. and I.Y.K.; project administration, I.Y.K. and M.V.K.; funding acquisition, I.Y.K. All authors have read and agreed to the published version of the manuscript.

Funding: The study is supported by the State Assignment for the Institute of Silicate Chemistry of the Russian Academy of Sciences (State registration numbers 0081-2022-0007 and 0081-2022-0003).

Institutional Review Board Statement: Not applicable.

Informed Consent Statement: Not applicable.

Data Availability Statement: Not applicable.

Acknowledgments: The authors are thankful to Anastasia Kovalenko (Institute of Silicate Chemistry of the Russian Academy of Sciences) for the assistance with dynamic pH-metry characterization of the studied materials.

Conflicts of Interest: The authors declare no conflict of interest.

References

1. Maric, R.; Mirshekari, G. *Solid Oxide Fuel Cells, From Fundamental Principles to Complete Systems*; CRC Press: Boca Raton, FL, USA, 2021; p. 256. [CrossRef]
2. Ponomareva, A.A.; Ivanova, A.G.; Shilova, O.A.; Kruchinina, I.Y. Current state and prospects of manufacturing and operation of methane-based fuel cells (review). *Glass Phys. Chem.* **2016**, *42*, 1–19. [CrossRef]
3. Ponomareva, A.; Babushok, V.; Simonenko, E.; Simonenko, N.; Sevast'janov, V.; Shilova, O.; Kruchinina, I. Influence of pH of solution on phase composition of samarium-strontium cobaltite powders synthesized by wet chemical technique. *Sol-Gel Sci. Technol.* **2018**, *87*, 74–82. [CrossRef]
4. Galushko, A.S.; Panova, G.G.; Ivanova, A.G.; Masalovich, M.S.; Zagrebelnyy, O.A.; Kruchinina, I.Y.; Shilova, O.A. An Overview of the Functional Ceramic and Composite Materials for Microbiological Fuel Cells. *J. Ceram. Sci. Technol.* **2017**, *8*, 433–454. [CrossRef]
5. Pachauri, Y.K.; Chauhan, R.P. A study, analysis and power management schemes for fuel cells. *Renew. Sustain. Energy Rev.* **2015**, *43*, 1301–1319. [CrossRef]
6. Rekas, M. Electrolytes for intermediate temperature solid oxide fuel cells. *Arch. Metall. Mater.* **2015**, *60*, 891–896. [CrossRef]
7. Mahato, N.; Banerjee, A.; Gupta, A.; Omar, S.; Balani, K. Progress in material selection for solid oxide fuel cell technology: A review. *Prog. Mater. Sci.* **2015**, *72*, 141–337. [CrossRef]
8. Sal'nikov, V.V.; Pikalova, E.Y. Raman and impedance spectroscopic studies of the specific features of the transport properties of electrolytes based on CeO_2. *Phys. Solid State* **2015**, *57*, 1944–1952. [CrossRef]
9. Egorova, T.L.; Kalinina, M.V.; Simonenko, E.P.; Simonenko, N.P.; Shilova, O.A.; Sevastyanov, V.G.; Kuznetsov, N.T. Liquid-Phase Synthesis and Physicochemical Properties of Xerogels, Nanopowders and Thin Films of the CeO_2–Y_2O_3 System. *Russ. J. Inorg. Chem.* **2016**, *61*, 1061–1069. [CrossRef]
10. Ramos-Alvarez, P.; Villafuerte-Castrejón, M.E.; González, G.; Cassir, M.; Flores-Morales, C.; Chávez-Carvayar, J.A. Ceria-based electrolytes with high surface area and improved conductivity for intermediate temperature solid oxide fuel cells. *J. Mater. Sci.* **2017**, *52*, 519–532. [CrossRef]
11. Trovarelli, A. Catalysis by ceria and related materials. *Catal. Sci. Ser. L. Imp. Coll. Press* **2002**, *2*, 528.
12. Kuznetsova, T.G.; Sadykov, V.A. Specific features of the defect structure of metastable nanodisperse ceria, zirconia, and related materials. *Kinet. Catal.* **2008**, *49*, 840–858. [CrossRef]
13. Jud, E.; Gauckler, L.-J. The effect of cobalt oxide addition on the conductivity of $Ce_{0.9}Gd_{0.1}O_{1.95}$. *J. Electroceram.* **2005**, *15*, 159. [CrossRef]
14. Tian, C.; Chan, S.-W. Ionic Conductivities, Sintering Temperatures and Microstructures of Bulk Ceramic CeO_2 Doped with Y_2O_3. *Solid State Ion.* **2000**, *134*, 89–102. [CrossRef]
15. Moghadasi, M.; Du, W.; Li, M.; Pei, Z.; Ma, C. Ceramic binder jetting additive manufacturing: Effects of particle size on feedstock powder and final part properties. *Ceram. Int.* **2020**, *46*, 16966–16972. [CrossRef]
16. Fathy, A.; Wagih, A.; Abu-Oqail, A. Effect of ZrO_2 content on properties of Cu-ZrO_2 nanocomposites synthesized by optimized high energy ball milling. *Ceram. Int.* **2019**, *45*, 2319–2329. [CrossRef]
17. Li, Z.; He, Q.; Xia, L.; Xu, Q.; Cheng, C.; Wang, J.; Ni, M. Effects of cathode thickness and microstructural properties on the performance of protonic ceramic fuel cell (PCFC): A 3D modelling study. *Int. J. Hydrog. Energy* **2022**, *47*, 4047–4061. [CrossRef]
18. Khasanov, O.L.; Dvilis, E.S.; Bikbaeva, Z.G. *Methods of Compacting of Nanostructured Materials and Articles*; Tomsk University: Tomsk, Russia, 2008; 212p. (In Russian)
19. Shilova, O.A.; Antipov, V.N.; Tikhonov, P.A.; Kruchinina, I.Y.; Panova, T.I.; Morozova, L.V.; Moskovskaya, V.V.; Kalinina, M.V.; Tsvetkova, I.N. Ceramic nanocomposites based on oxides of transition metals of ionistors. *Glass Phys. Chem.* **2013**, *39*, 570–578. [CrossRef]
20. Rempel, A.A.; Gusev, A.I. *Nanocrystalline Materials*; Cambridge International Science Publishing: Cambridge, UK, 2004; p. 351. ISBN 978-1-898326-26-7.
21. Lyagaeva, Y.G.; Medvedev, D.A.; Demin, A.K.; Yaroslavtseva, T.V.; Plaksin, S.V.; Porotnikova, N.M. Specific features of preparation of dense ceramic based on barium zirconate. *Semiconductors* **2014**, *48*, 1353–1358. [CrossRef]
22. Duran, P.; Villegas, M.; Capel, F.; Recio, P. Low temperature sintering and microstructural development of nanocrystalline Y-TZP ceramics. *J. Eur. Ceram. Soc.* **1996**, *16*, 945–952. [CrossRef]
23. *GOST 473.4-81*; Vanadium Base Alloys and Alloying Elements. Methods for Determination of Silicon. GOST Russian Standard: Moscow, Russia, 1981. (In Russian)
24. Sergey, V.M.; Maxim, M.S.; Inna, V.V. (Eds.) *Electron Beam Modification of Solids: Mechanisms, Common Features and Promising Applications*; Nova Science Publishers, Inc.: Hauppauge, NY, USA, 2009; ISBN 978-1-60741-780-4.

25. Fedorenko, N.Y.; Mjakin, S.V.; Khamova, T.V.; Kalinina, M.V.; Shilova, O.A. Relationship among the Composition, Synthesis Conditions, and Surface Acid-Basic Properties of Xerogel Particles Based on Zirconium Dioxide. *Ceram. Int.* **2022**, *48*, 6245–6249. [CrossRef]
26. Pivovarova, A.P.; Strakhov, V.I.; Popov, V.P. On the mechanism of electron conductivity in lanthanum metaniobate. *Tech. Phys. Lett.* **2002**, *28*, 815–817. [CrossRef]